FLOW PREDICTION IN A BLOWER CASING

HORIA DUMITRESCU[*], VLADIMIR CARDOŞ[*]

Using the assumption of inviscid and irrotational flow, a singularity method for computing the flow field in a radial-flow blower is presented. For a particular example, the influence of the geometry of the blower casing on the flow field in the casing is investigated. The details of the flow at the impeller outlet are analyzed. The circumferential inhomogeneity of the flow properties at the impeller outlet suggests that vorticity and fluid viscosity may play an important role for the flow behaviour in the blower.

1. INTRODUCTION

The discharge casing is that part of the casing following the impeller outlet. It has two functions: (1) to receive and guide the fluid discharged from the impeller to the outlet part of the blower and (2) to increase the static head at the outlet of the blower by reducing the kinetic energy of the fluid leaving the impeller. These two functions are called collector and diffuser functions. The former function may be used alone while the latter can occur either before or after the collector function. In addition diffusion can take place in a vaned or vaneless diffuser. A simple volute or scroll collector is illustrated in Fig. 1 and consists of a circular passage of increasing cross-sectional area. The advantage of the simple volute is its low cost and its designing is a significant task.

In the absence of the casing the streamlines of the free vortex absolute flow at the impeller outlet follow logarithmic spiral lines. Thus the casing of radial-flow blowers should be approximately like such a logarithmic spiral shape for providing equal pressures around the blower casing, and hence no radial thrust on the shaft. However, because the angle of the volute, *i.e.* the constant angle made by the volute with radial lines, depends on the tangential to radial absolute velocity component ratio, the volute casing is limited to operation efficiently at the fixed design point. For the other operating points the flow in the casing deviates less or more from the ideal logarithmic spiral streamlines. Moreover, even at the design operating point can appear significant deviations from the ideal streamlines due to the rounded shape of the volute tongue that does not permit to be sufficiently close

[*] "Caius Iacob " Institute of Applied Mathematics, P.O. Box 1–24, RO-707000, Bucharest
[**] "Valahia" University of Târgovişte

Rev. Roum. Sci. Techn. – Méc. Appl., Tome 52, N^o 3, P. 173–189, Bucarest, 2007

to the impeller outlet. Any deviation in flow rate from the design condition will result in a radial thrust, which if allowed to persist could result in shaft bending.

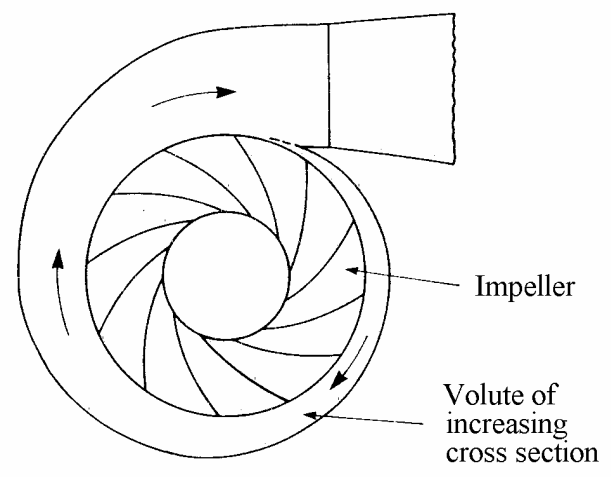

Fig. 1 – Simple volute or scroll collector.

Recently, large progress has been made in the mathematical modeling of flow processes in fluid machines. This progress not only can be seen in the field of sophisticated methods based on Euler and Navier-Stokes equations [1], but also in the field of simple two-dimensional calculation methods [2–4]. This progress is mainly due to the increasing efforts to expand the use of computers in the design of fluid machines. For rather simple fluid machines like centrifugal fans and pumps, nowadays, the two-dimensional calculation methods for the prediction of the performance have obtained a degree of accuracy that allows them to be used in an inverse way as a design tool.

The present paper describes a plane two-dimensional flow analysis for a concrete example of radial-flow blower casing. The main aim was to investigate the influence of the geometry of the blower casing on the flow field behind the impeller. Particularly, the details of the circumferential inhomogeneity of the flow properties at off-design conditions are discussed. In the theoretical considerations that follow next, it assumes that the flow in casing between the impeller outlet and machine outlet is a free vortex flow that can be approximated for a constant width of volute by a two-dimensional potential flow. However, it appears that vorticity and fluid viscosity, neglected in modelling, have important implications for flow behaviour in the blower.

2. FLOW ANALYSIS

Physics of the flow and model development. Without casing the free absolute flow downstream of the impeller can be approximated by the two-dimensional potential flow produced by a point source and point vortex placed at the origin of coordinates in the physical plane, $z(=re^{i\varphi})$. Considering such a source-vortex combination of strength Q_0 and Γ_0, respectively, at the origin, the complex potential for this flow is

$$f(z)=\frac{Q_0-i\Gamma_0}{2\pi}\ln z\,. \tag{1}$$

The strengths of the source and vortex can be obtained from the volume width unity-flow rate at the impeller outlet and the circulation around the impeller periphery as

$$Q_0=\frac{Q}{b_2}=r_2\int_0^{2\pi}C_{n2}(\theta)\mathrm{d}\theta=2\pi r_2\overline{C}_{n2}\,, \tag{2}$$

$$\Gamma_0=r_2\int_0^{2\pi}C_{u2}(\theta)\mathrm{d}\theta=2\pi r_2\overline{C}_{u2}\,, \tag{3}$$

where r_2 and b_2 are the impeller outlet radius and width, and C_{n2}, C_{u2}, $\overline{C}_{n2}$, $\overline{C}_{u2}$ are the local and average values of the radial and tangential absolute velocity components at the impeller outlet, respectively.

The streamlines due to a source-vortex superposition at the origin are logarithmic spiral lines that can approximate both the impeller blades cascade and absolute flow at the impeller outlet. The circular cascade on the z – plane can be conformally transformed into a straight cascade on the z' – plane by the use of the conformal function

$$z'=K\ln\frac{z}{\sqrt{r_1r_2}}\,, \tag{4}$$

where N is the number of blades and $K=\frac{Nt}{2\pi}e^{-i\alpha'}$. As shown in Fig. 2, the straight cascade (z' – plane), whose pitch and angle are t and α', respectively, is placed in the uniform flow with velocity U_∞. The velocity potential for this case will be

$$F(z')=U_\infty z'\,. \tag{5}$$

Equating the two expressions of the velocity potential, eqs. (1) and (5), for the equal flow rate and circulation around airfoil in the two plane, it results in the mapping function, eq. (4).

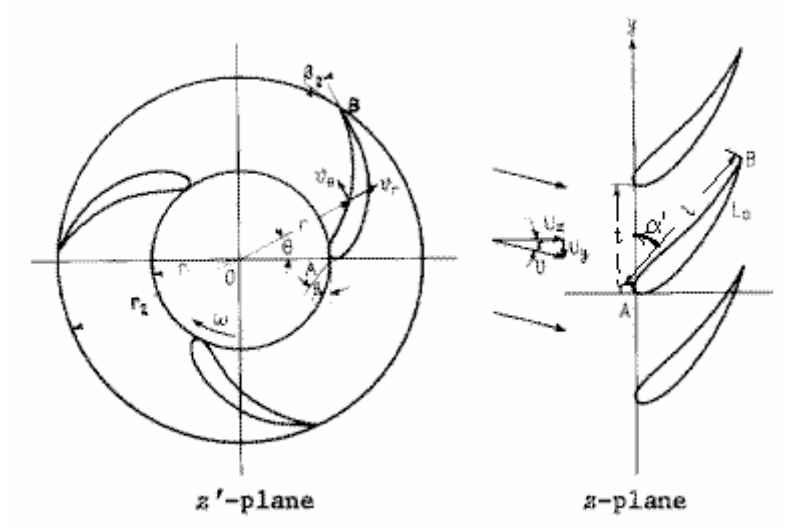

Fig. 2 – Physical plane and mapped plane.

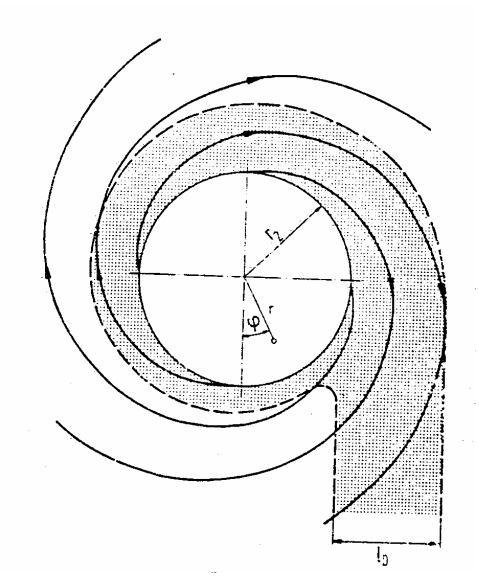

Fig. 3 – Streamlines for $T = 5$.

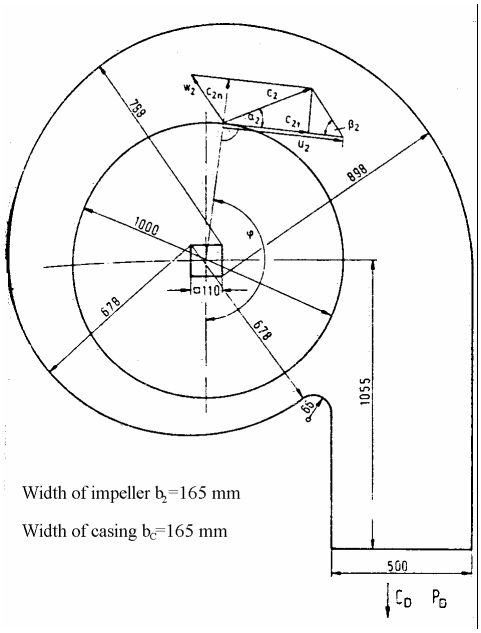

Fig. 4 – Spiral casing.

For an incompressible fluid, the inclination of the absolute velocity vector to the radial line remains constant at all θ since at the outlet from the impeller

$$\tan\alpha' = \tan\alpha'_2 = \overline{C}_{u2} / \overline{C}_{n2} = \frac{\Gamma_0}{Q_0} = T\,, \tag{6}$$

since rC_n is constant from the constant mass flow rate requirement, and rC_u is constant from the conservation of angular momentum requirement. Thus the flow downstream of the impeller remains at a constant inclination α' to radial lines, the flow path tracing out a logarithmic spiral

$$\theta - \theta_2 = T \ln(r / r_2), \tag{7}$$

where T is a parameter of the source-vortex coupling called twist coefficient.

Figure 3 shows streamlines for $T = 5\left(\alpha'_2 = 78.7^0\right)$. To analyze the flow in casing we consider a particular example shown in Fig. 4, that corresponds approximately to a logarithmic spiral casing with $\alpha_2 = 6.5^0 (T = 9.8)$ and a width equal to that of the impeller at outlet, $b_0 = b_2$. A different value for the casing width can be taken into account by changing the twist coefficient. The flow field between impeller outlet (subscript 2) and machine outlet (subscript 0) is assumed plane two-dimensional potential one, and subjected to the following boundary conditions:

a) Constant velocity in cross-sectional area of flow at the outlet port

$$C_0 = \frac{Q}{b_2 h_0} = \overline{C}_{n2} \frac{2\pi r_2}{h_0}, \tag{8}$$

where h_0 is the height of outlet part.

b) The casing contour is one of streamlines of the absolute flow.

c) Different boundary conditions can be imposed at the impeller outlet, as it follows:

1) a radial velocity distribution, $C_{n2}(\theta)$, that satisfies eq. (2);

2) a tangential velocity distribution, $C_{u2}(\theta)$, that satisfies eq. (3);

3) a combination of both radial and tangential velocity distributions, $C_{n2}(\theta)$ and $C_{u2}(\theta)$, that satisfies the constant flow angle requirement

$$\tan\alpha_2 = \frac{C_{n2}(\theta)}{C_{u2}(\theta)} = \text{constant}\,; \tag{9}$$

4) a constant pressure around the contour $r = r_2$ requirement, $p_2 =$ = constant condition expressed as

$$C_2^2 = C_{n2}^2(\theta) + C_{n2}^2(\theta) = \text{constant}\,. \tag{10}$$

In the absence of the casing, the absolute flow at the outlet from the impeller is axisymmetric and all the above conditions are automatically satisfied. When the

flow is enclosed by a casing, care must be taken to ensure suitable boundary conditions at the impeller outlet. Because these conditions are not a priori known, different conditions at the impeller outlet will be analyzed next and their results will be compared.

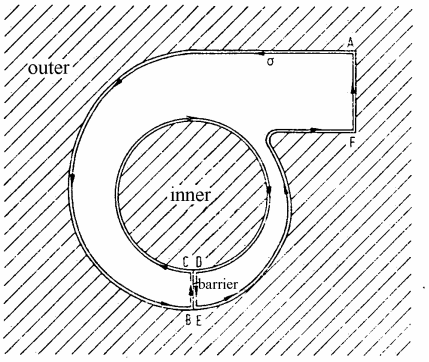

Fig. 5 – Flowfield domain.

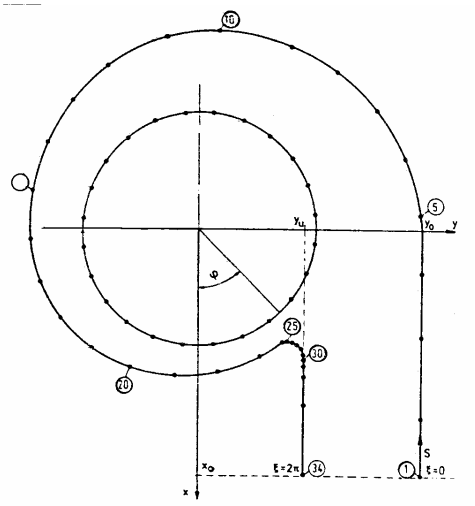

Fig. 6 – Distribution of the computation points along the casing and impeller contours.

Singularity method. Now consider irrotational motion in the doubly connected region exterior to an impeller as shown in Fig. 5. Inserting a barrier as shown in the figure a simply connected region is obtained. Consider the curve that consists of C_I and C_C, which surround the impeller, casing and the two sides of the barrier. Since the region excluding the barrier is simply connected, the integration of an analytic function *f(z)* around this curve is zero

$$\oint_{C_C} f(z)\mathrm{d}z - \oint_{C_I} f(z)\mathrm{d}z = 0\,. \tag{10}$$

Note that the first term is the integral around C_C (casing contour) and the second is minus the integral around C_I (impeller contour). The contributions from barrier cancel for steady flow.

The application of surface singularity methods allows the treatment of more realistic geometries and the fulfillment of the boundary conditions on the actual surface. Thus, the potential flow past a body placed in a uniform stream can be modeled by replacing the body surface with source and vortex singularities. Integral equations can then be written expressing the Neumann boundary condition of zero normal surface velocity for the source model or the Dirichlet condition of

zero parallel surface velocity for the vorticity model. Whichever type of singularity is chosen the final outcome is the same namely a prediction of the potential flow velocity close to the body profile. In the present singularity method the impeller and region exterior to the casing surround the inner region when the flow of interest occurs. The solution for this flow can be obtained by distributing elementary singular solutions (sources and vortices) on the inner region boundaries (C_C, C_I). The singularity distribution strengths (σ, γ) are determined by specifying the previous boundary conditions at the collocation points selected on the contour ($C_C + C_I$). Martensen's boundary integral formulation [5] based on a surface vorticity distribution (γ) is used to obtain the solution of this problem. The Martensen method has the advantage that the potential flow velocity close to the body surface is exactly equal to the surface vorticity.

Equating the circulation around a contour surrounding a small vorticity element γds, defined clockwise positive, with the total amount of vorticity enclosed by the contour, it can obtain

$$\gamma = v_{t_0} - v_{t_i}, \tag{11}$$

where v_{t_0} and v_{t_i} are the fluid velocities just outside hatched region in fig.5 and inside the vortex sheet, which must be parallel to the body surface. The velocities on the two sides of the vortex sheet are given respectively by the

$$v_{t_0} = v_t + \gamma/2, \tag{12}$$

$$v_{t_i} = v_t - \gamma/2, \tag{13}$$

where $v_t = \left(v_{t_0} + v_{t_i}\right)/2$ is the tangential velocity component induced by all singularities distributed along the inner region contour, except the singularity placed at the computation point. The similar relationships can be obtained for a surface source distribution (σ) and the normal velocity component (defined outside the inner region-positive).

$$\sigma = v_{n_0} - v_{n_i}, \tag{14}$$

$$v_{n_0} = v_n + \sigma/2, \tag{15}$$

$$v_{n_i} = v_n - \sigma/2, \tag{16}$$

where $v_n = \left(v_{n_0} + v_{n_i}\right)/2$ is the normal velocity component induced by singularities. The condition of zero velocity inside the outer region, $v_{t_0} = v_{n_0} = 0$, leads to

$$\gamma = -v_{t_i}, \quad \gamma/2 = -v_t, \tag{17}$$

$$\sigma = -v_{n_i}, \quad \sigma/2 = -v_n . \tag{18}$$

Formulation of governing equations. Applying the foregoing arguments, we may represent this flow by a vortex distribution, γ, along the casing contour, source and vortex distributions, σ_I and γ_I, along the impeller contour and a uniform source distribution at the outlet part of the blower, $\sigma_0 = -c_0$, assuming to be sufficiently away downstream of the impeller. To find the unknown singularity distributions, according to Eqs. (17) and (18), the casing and impeller contour is described by the parametric formulae

$$x_c = f_1(\xi), \quad y_c = f_2(\xi), \tag{19}$$

$$x_I = r_2 \cos\theta, \quad y_I = r_2 \sin\theta, \tag{20}$$

where the parameters ξ and θ take values from 0 to 2π, and f_1, f_2 are spline type functions which carry out a correspondence between a number of points nonuniforn distributed along the casing contour and the points of the equidistant scale ξ. The casing contour must be divided especially finely at the part where the curvature is fairly large.

The parametric representation of the boundary contour allows a parametric description of the velocity field

$$v_t = \vec{v}_{is}\vec{t} = \left(-u\dot{x} - v\dot{y}\right)/\sqrt{\dot{x}^2 + \dot{y}^2}, \tag{21}$$

$$v_n = \vec{v}_{is}\vec{n} = \left(u\dot{y} - v\dot{x}\right)/\sqrt{\dot{x}^2 + \dot{y}^2}, \tag{22}$$

where $\vec{t}$ is tangent to contour, $\vec{n}$ is the outward normal to contour and $\vec{v}_{is}(u,v)$ is the induced velocity vector by singularities.

Introducing the computation parameters defined as

$$\begin{aligned} w_{tC} &= \gamma_C \sqrt{\dot{x}_C^2 + \dot{y}_C^2}, \\ w_{tI} &= \gamma_I \sqrt{\dot{x}_I^2 + \dot{y}_I^2}, \\ w_{nI} &= \sigma_I \sqrt{\dot{x}_I^2 + \dot{y}_I^2}, \end{aligned} \tag{23}$$

and making use of the equations (17) and (18), the Dirichlet boundary condition of zero velocity on (and tangent to) the boundary contour may then be expressed as:

$$\pi w_{tC} - \int_0^{2\pi} E_{CC} w_{tC}(\xi')\mathrm{d}\xi' = \int_0^{2\pi} E_{CI} w_{tI}(\theta')\mathrm{d}\theta' + \int_0^{2\pi} F_{CI} w_{nI}(\theta')\mathrm{d}\theta' + \int_{y_d}^{y_u} F_{CO}\sigma_O(y')\mathrm{d}y', \tag{24}$$

$$\pi w_{tI} - \int_0^{2\pi} E_{CC} w_{tI}(\theta')\,\mathrm{d}\theta' = \int_0^{2\pi} E_{CI} w_{tC}(\xi')\,\mathrm{d}\xi' + \int_0^{2\pi} F_{II} w_{nI}(\theta')\,\mathrm{d}\theta' + \int_{y_d}^{y_u} F_{IO}\sigma_O(y')\,\mathrm{d}y', \quad (25)$$

$$\pi w_{nI} + \int_0^{2\pi} H_{II} w_{nI}(\theta')\,\mathrm{d}\theta' = -\int_0^{2\pi} G_{CI} w_{tC}(\xi')\,\mathrm{d}\xi' - \int_0^{2\pi} G_{II} w_{tI}(\theta')\,\mathrm{d}\theta' - \int_{y_d}^{y_u} H_{IO}\sigma_O(y')\,\mathrm{d}y', \quad (26)$$

where E_{ij}, F_{ij}, G_{ij} and H_{ij} may be called the geometric influence coefficients which present the magnitude of the effect of the singularity (source and vortex) at (x'_j, y'_j) upon the point (x_i, y_i) and are defined as

$$\begin{aligned}
E_{ij} &= \frac{(y_i - y'_j)\dot{x}_i - (x_i - x'_j)\dot{y}_i}{(x_i - x'_j)^2 + (y_i - y'_j)^2},\\
F_{ij} &= \frac{(x_i - x'_j)\dot{x}_i + (y_i - y'_j)\dot{y}_i}{(x_i - x'_j)^2 + (y_i - y'_j)^2},\\
G_{ij} &= \frac{(y_i - y'_j)\dot{y}_i + (x_i - x'_j)\dot{x}_i}{(x_i - x'_j)^2 + (y_i - y'_j)^2},\\
H_{ij} &= \frac{(x_i - x'_j)\dot{y}_i - (y_i - y'_j)\dot{x}_i}{(x_i - x'_j)^2 + (y_i - y'_j)^2}.
\end{aligned} \quad (27)$$

The subscripts *C*, *I* and *O* used in Eqs. (24)–(26) represent conditions at the casing contour, impeller circumference and outlet port, respectively.

Equations (24)–(26) are Martensen's boundary integral formulation for plane two-dimensional flow considered here and they are Fredholm integral equations of the second kind. Compared with same other singularity methods it offers the special advantage that its kernel is non-singular and thus the derivation of numerical solutions is extremely straightforward.

The simultaneous equations (24)–(26) are coupled by the boundary conditions, Eqs. (8–10) must be satisfied. For the zero circulation flow case, $T = 0,\ w_{nI} = \text{const.}$ and Eq. (26) is selfsatisfied, while for the zero mass flow rate case, $T = \infty,\ w_{tI} = \text{const.}$ and Eq. (25) is selfsatisfied. For other values of the twist coefficient, the solution results from superimposing these two basic solutions. Since the flow angle α must be constant, then

$$\tan\alpha_2 = w_{nC} / w_{tC} = \text{const.} \quad (28)$$

and eqs. (25) and (26) can be added. For the constant pressure case, p_2 = const., the solutions is computed employing an iterative method.

3. RESULTS AND DISCUSSION

In order to check the validity of the just described model; it is essential to compare its predictions obtained for different boundary conditions. For numerical computations a concrete casing geometry was chosen. The computation point distribution along the casing contour is shown in Fig. 6.

Velocity and pressure distributions on the flow field boundary. Figures 7–10 present the distributions of radial and tangential absolute velocity components $C_{2n}(\theta)/\overline{C}_{2n}$, $C_{2t}(\theta)/\overline{C}_{2n}$, pressure coefficient $C_p(\theta)=\dfrac{p_2(\theta)-p_0}{\rho C_0^2/2}$, and flow angle α_2, around the periphery of the impeller, for four different boundary conditions. These figures show that for all boundary conditions does exist significative deviations from the average values of quantities. There are also significant differences among the predictions corresponding to the different boundary conditions. The velocity distribution around the casing contour for the same boundary conditions at the impeller outlet is shown in Fig. 11. As seen in this figure, close to the tangue the slope of the velocity distribution along the casing contour becomes steep for all cases presented.

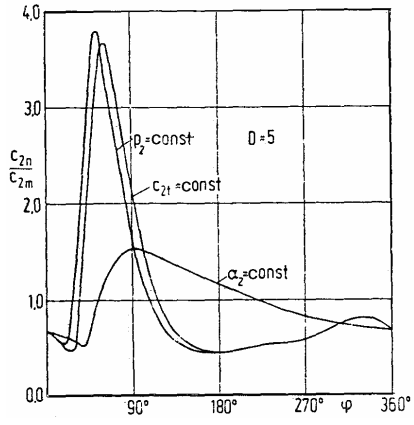

Fig. 7 – Radial velocity distribution for different boundary conditions at the impeller outlet.

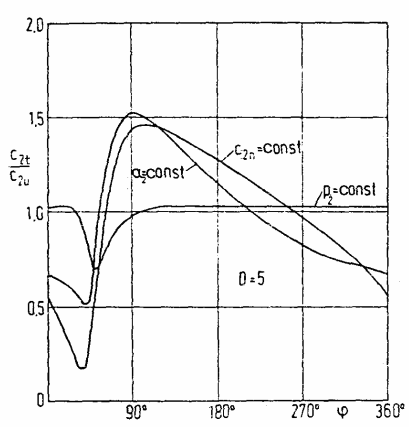

Fig. 8 – Tangential velocity distribution for different boundary conditions at the impeller outlet.

From the four different boundary conditions considered here, the constant flow angle condition (α_2 = const.) seems to be the most plausible since the flow direction is physically prescribed by the impeller blades (Fig. 7). Figures 8 and 9 show that predicted values of the tangential velocity component and pressure coefficient with C_{n2} = const. (first boundary condition) are very close to those

obtained with the best condition, $\alpha_2 = \text{const}$. The influence of the tongue tends to give a kind of irregularity to curves, occurring large deviations as against the average values (50%–80% for tangential velocity component and more than 100% for pressure coefficient). At the design point, the characteristic curve (Fig. 18) gives the total head developed by the blower for $T = 5$

$$\frac{p_0 - p_I}{\rho C_0^2 / 2} = \Psi / \Phi^2 = 2.7\,, \tag{29}$$

where p_I and p are the pressures at the inlet and outlet ports, respectively, Ψ is the head coefficient, and Φ is the flow coefficient. As shown in Fig. 9, the deviation of pressure along the impeller contour represents approximately 50% from the total head developed by the blower. Therefore, it is clearly visible the necessity to draw as accurate as possible the contour of casing.

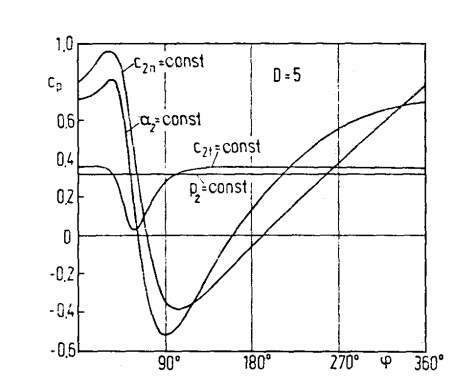

Fig. 9 – Pressure coefficient distribution for different boundary conditions at the impeller outlet.

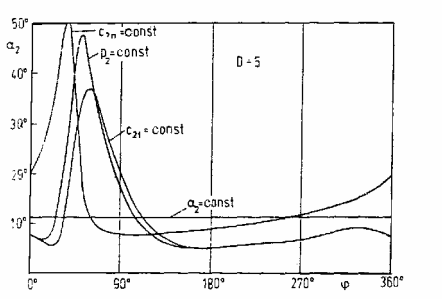

Fig. 10 – Flow angle distribution at impeller outlet for different boundary conditions.

Effect of tongue shape. Because steep variations of flow variables occur on both impeller and casing contour in the tongue zone (points 25–30), it is to be expected the curvature radius (R_t) of tongue to have certain influence. To make visible this effect the distribution of tangential velocity component along the impeller contour and the velocity distribution on the casing contour have been plotted for values of curvature radius R_t varying from 55 mm to 88 mm, with $T = 4.4$ and $C_{n2} = \text{const}$. condition (Figs. 12 and 13). Though it notes some differences the curvature of tongue has slight influence in the presented cases.

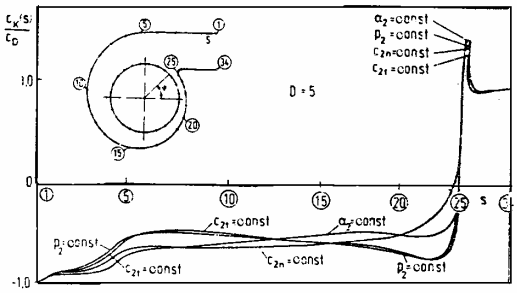

Fig. 11 – Velocity distribution along the casing contour
for different boundary conditions
at the impeller outlet.

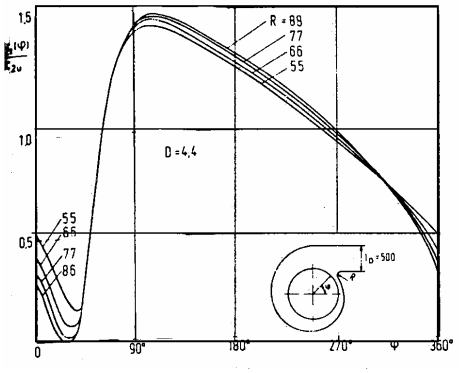

Fig. 12 – Tangential velocity distribution along the
impeller contour for different curvature radii
of the tongue (with c_{2n} = const.).

Twist effect. The twist coefficient was varied in large limits, from $T = 0$ (zero circulation) to $T = \infty$ (zero mass flow rate) and the velocity distribution along the impeller and casing contour have been plotted and compared. The values of $C_{2n}(\theta)/\overline{C}_{2n}$, $C_{2t}(\theta)/\overline{C}_{2n}$ and C_C / C_O calculated with p_2 = const. condition are compared in Figs. 14, 15 and 16 only for two values of T, 5 and 10. A reduction of irregularity to the curves of the normal and tangential velocity components on the impeller contour can be observed for T=10. For values less than the optimum twist the irregularity to the curves of velocities on the impeller contour tends to concentrate strongly in the tongue zone ($30\,\text{deg.} \le \theta \le 90\,\text{deg.}$). The influence of twist on the tangential velocity distribution is much less than for the normal velocity. Predictions for the velocity distribution on the casing contour are compared in Fig. 16, for two values of twist.

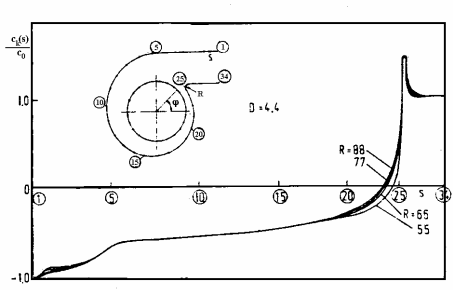

Fig. 13 – Velocity distribution along the casing cotour for different curvature radii of the tongue (with c_{2n} = const.).

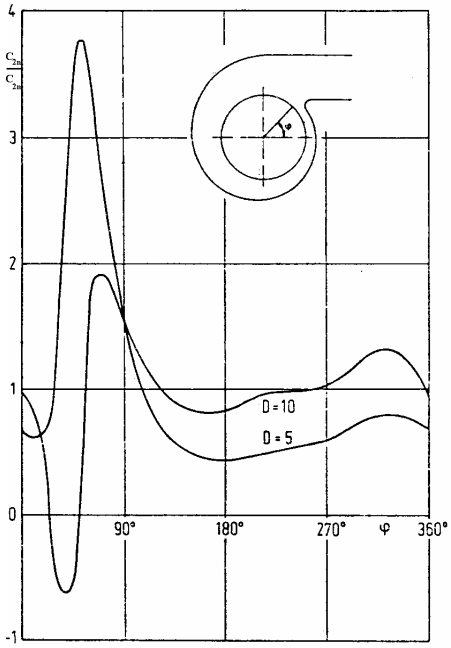

Fig. 14 – Radial velocity distribution along the impeller contour for different twist coefficients (with p_2 = const.).

Effect of twist on characteristic curve. For the ideal impeller with infinite number of blades closely spaced the relative velocity vector at outlet is tangent to the blade, this being set at angle β_2 from the tangential direction. Figure 17 shows the velocity triangle drawn at outlet for analyzed case (U_2 = 78.5 m/s, β_2 = 30 deg.). By subtracting the impeller outlet tangential velocity U_2, the absolute velocity vector C_2 is obtained, this being set at angle α_2 from the tangent to the blade. Then, the tangential component of absolute velocity is given by

$$C_{u2} = U_2 - \overline{C}_{n2} \tan^{-1} \beta_2 . \tag{30}$$

Due to the finite number of blades (Z = finite number), in both centrifugal pumps and blowers it occurs a fluid slip, which manifests itself as a reduction in tangential component C_{u2}. After reference [6] this component can be calculated as

$$C'_{u2} = C_u^2 \left\{1 + (1.5/Z)\left[1 + (\beta_2 / 60\,\text{deg.})\right] / \left[1 - (r_1 / r_2)^2\right]\right\}^{-1} . \tag{31}$$

For the present particular case with Z=6, $r_1 / r_2 = 0.56$, $\beta_2 = 30^{\circ}$ it obtains

$$C'_{u2} = 0.65 C_{u2}, T = C'_{u2} / \overline{C}_{n2} = 0.65\left(\frac{2\pi}{\Phi} - 1.732\right), \tag{32}$$

where $\Phi = Q/(A_0 u_2)$ is the flow coefficient.

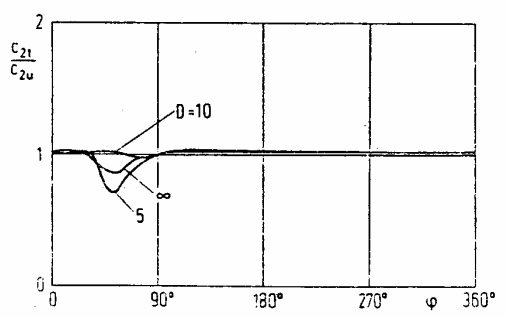

Fig. 15 – Tangential velocity distribution along the impeller contour for different twist coefficients (with p_2 = const.).

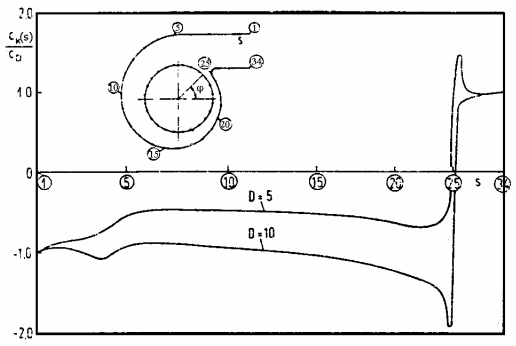

Fig. 16 – Velocity distribution along the casing contour for two values of twist coefficient (with p_2 = const.).

Figure 18 represents the head coefficient Ψ as a function of the flow coefficient Φ and the real twist coefficient, for equal width of impeller and casing. However, the characteristic in figure was measured for a width ratio $b_2 / b_c = 0.412$ [7], so that the twist coefficient is

$$T_e = T b_2 / b_c . \tag{33}$$

The optimum value of the twist coefficient results from

$$T_{opt} = \tan^{-1} \alpha_{opt} \frac{b_2}{b_c}, \tag{34}$$

where α_{opt} corresponds to operation at the maximum efficiency point (here $T_{opt} = 3.9$). The computations have demonstrated that the most reduced irregularities to the curves of flow variables on the impeller contour occur for the twist coefficient corresponding to the maximum efficiency.

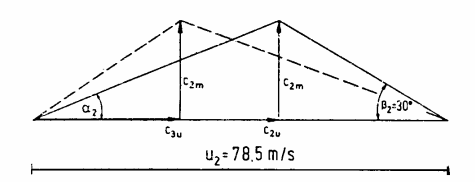

Fig. 17 – Velocity triangles.

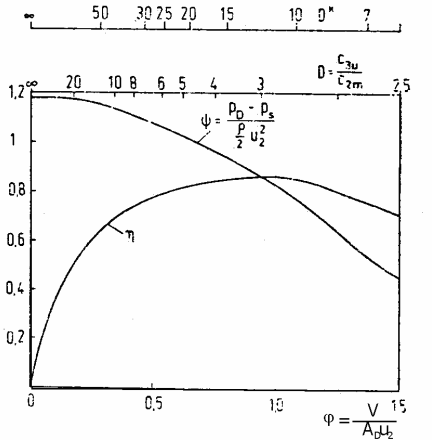

Fig. 18 – Measured efficiency and head coefficient curves as a function of flow coefficient.

Effect of flow nonuniformity in outlet port. The casing flow model previously developed was based on the assumptions of potential flow (inviscid and irrotational motion) and uniform velocity in cross-sectional area at outlet. Even if the flow model is simplified one, however this allows one to have an idea about the strongly irregular variations on the impeller contour, resulting in an increase of the pressure on contour, a rotational flow and a non-uniform velocity and pressure in cross-sectional area of the outlet port (pressure at point 34 is much higher than pressure at point 1). Generally speaking, the irrotational flow model reproduces quite well the motion of the fluid leaving the impeller at $\theta \geq 90$ deg. Only this inviscid and irrotational fluid with low pressure leaves for outlet and arrives at point 34 increasing its static head and reducing its kinetic energy due to the volute geometry of casing. A more regular pressure distribution on the impeller contour resulting in a static head increase for $\theta \geq 90$ deg. and a corresponding velocity increase at point 34 seems to be achieved if a rotational flow were assumed. The flow vorticity has an uniformity effect on the velocity and pressure distributions at outlet. Actually

the flow in impeller and casing is both viscous and irrotational resulting in flow separation at walls and a swirling secondary flow arising from the curved surfaces. This secondary flow induces a large nonuniformity of the velocity distribution in cross sectional area of the outlet port (velocity at top (point 1) is higher than at bottom (point 34)). Though the effects of vorticity and viscosity on the flow uniformity are contrary, the destabilizing effect of viscosity prevails.

Analysis of computed results presented in the previous section has demonstrated the significant effect of casing shape on the behaviour of flow both in machine and in outlet port. A well shaped casing smoothes the pressure irregularities around the periphery of the impeller, resulting in equal pressures around the blower casing, and hence no radial thrust on the shaft. A simple volute casing was chosen for the numerical application, though also other casing geometries can be imaged which to fulfil the uniform flow at outlet requirement.

4. CONCLUSIONS

The main objective of this study was to develop a method to analyze the flow in a radial-flow blower casing. This method has the following characteristics. The flow in the volute casing is assumed to be plane two-dimensional potential one and Martensen's singularity method is used. The vortices and sources were distributed on the impeller and casing contour, at midpoints of the divided segments and the equations (24)–(26) could be expressed as linear equations. By this method even when the casing contour was divided into unequal segments, the velocity distribution could be computed accurately and the number of the unknowns of simultaneous linear equations could be kept small and consequently a large computer was not necessary. A peculiar investigation was carried out on boundary conditions at the impeller outlet.

In this paper, though the theoretical results were presented for only one kind of casing shape, there was almost no restriction as for the casing shape.

Received 10 June 2002

REFERENCES

1. Y. TANIDA, M.NAMBA, *Unsteady aerodynamics and aeroelasticity of turbomachines*, Elsevier, Oxford, 1995.
2. R.I. LEWIS, *Vortex element methods for fluid dynamic analysis for engineering systems*, Cambridge University Press, Cambridge, 1991.
3. E. BONATAKI, P. CHAVIAROPOULOS, K.D. PAPAILIOU, *An inverse inviscid method for the design of quasi-three-dimensional turbomachinery cascades*, Journal of Fluids Engineering, **115**, *1*, 1993.

4. H. DUMITRESCU, V. CARDOŞ, *Flow prediction in a centrifugal impeller*, Rev. Roum. Sci. Techn. – Méc. Appl., **44**, *4*, 1999.
5. E. MARTENSEN, *Berechnung der Druckversteilung an Gitterprofilen in ebenor Potential strömung mit einer Fredholmschen Integralgleichung*, Arch. Rat. Mech., Anal., **3**, 1959.
6. C. PFLEIDERER, H. PETERMANN, *Strömungsmachinen*, Springer-Verlag, Berlin, 1964.
7. T. GIKADI, *Experimentalle Untersuchungen zum Einflu der Gehänseform auf die Strömung und das Strömungsgeräusch*, DFVLR-FB81-20, 1981.